European Journal of Immunology

Importance of antibody isotypes in anti-tumor immunity by monocytes and complement using human-immune tumor models

Sandra Lara[1], *Jessica C. Anania*[2,3], *Alexander Virtanen*[1], *Viktoria Stenhammar*[1], *Sandra Kleinau*[1]*

[1]Department of Cell and Molecular Biology, Uppsala University, Uppsala, Sweden.

[2]Department of Medical Biochemistry and Microbiology, Uppsala University, Uppsala, Sweden.

[3]Center for Cancer Immunology, University of Southampton, Southampton, UK.

*Corresponding author

Email: Sandra.Kleinau@icm.uu.se

Keywords: antibody-dependent phagocytosis (ADP), complement-dependent cytotoxicity (CDC), Rituximab, isotypes, human 3D tumor-immune model

Abstract

Monoclonal antibodies (mAb) have revolutionized clinical medicine, especially in the field of cancer immunotherapy. The challenge now is to improve the response rates, as immunotherapy still fails for many patients. Strategies to enhance tumor cell death is a fundamental aim, but relevant model systems for human tumor immunology are lacking. Herein, we have developed a pre-clinical human immune – three-dimensional (3D) tumor model (spheroids) to map the efficiency of tumor-specific isotypes for improved tumor cell killing. Different anti-CD20 Rituximab (RTX) isotypes alone or in combination, were evaluated for mediating complement-dependent cytotoxicity and antibody-dependent phagocytosis by human monocytic cells in 3D spheroids, in parallel with monolayer cultures,

Received: 07 14, 2020; Revised: 12 31, 2020; Accepted: MONTH DD, YYY

This article has been accepted for publication and undergone full peer review but has not been through the copyediting, typesetting, pagination and proofreading process, which may lead to differences between this version and the Version of Record. Please cite this article as doi: 10.1002/eji.202048885.

of human $CD20^+$ B-cell lymphomas. We demonstrate that the IgG3 variant of RTX has the greatest tumoricidal effect over other isotypes, and when combined with apoptosis-inducing RTX-IgG2 isotype the therapeutic effect can be substantially enhanced. The results show further that the treatment outcome by RTX isotypes is influenced by tumor morphology and expression of the complement inhibitor CD59. Hence, the human immune-3D tumor model is a clinical relevant and attractive *ex vivo* system to predict mAbs for best efficacy in cancer immunotherapy.

Introduction

Antibody-based immunotherapies are becoming the cornerstone treatment strategy for cancer. Therapeutic antibodies enable the patients' immune system to target, and destroy, the cancer cells. The potential impact of this treatment is huge, due to the highly specific nature of antibodies they have less side-effects than other treatments[1,2,3].Yet, our understanding of antibody-host interactions and immune functions dictating the quality of the tumor response after their administration is largely lacking. Strategies to enhance tumor cell death and tumor cell uptake is a fundamental aim, but for this relevant and predictive model systems for human tumor immunology are needed.

Antibodies have a dual activity inherent to their structure, where the two variable Fab regions bind to the antigen, while the Fc region activates the immune system. Thus, upon antibody binding to its target the Fc region can elicit numerous immune mediated functions including antibody- dependent phagocytosis (ADP), antibody- dependent cell- mediated cytotoxicity (ADCC) and complement- dependent cytotoxicity (CDC), all of which are essential for effective immunotherapy[4]. Their efficacy can be influenced by the percentage of target cells expressing the antigen, the density of antigen on the cell surface and the internalization rate, but also on the class of antibody administered. Accordingly, as the Fc region differs among different antibody isotypes it will impact complement activation and Fc receptor (FcR) binding on immune cells, hence each antibody isotype is functionality different. Current, therapeutic antibodies mainly use human IgG subclasses (IgG1, IgG2, IgG3 and IgG4), predominantly IgG1, as their backbone. These antibodies bind with different affinities to the three classes of FcR for IgG (FcγR); FcγRI (CD64), FcγRIIA, IIB, IIC (CD32A, B, C) and FcγRIIIA, IIIB (CD16A, B). All FcγRs deliver activating signals when aggregated by antibodies and antigens, except CD32B and CD32C, which transmit an inhibitory signal[5,6]. Myeloid cells, such as monocytes and macrophages, are superior for FcR-mediating effects as

they can express FcγRs CD64, CD32A, CD32B and CD16A, as well as the FcαR (CD89), hence mediate IgG and IgA effector functions, respectively[7]. CD89 promotes ADCC and ADP by engagement with either IgA subclass (IgA1, IgA2) in immune complexes, making IgA-based immunotherapy an underrepresented interesting avenue for future therapeutic mAbs[8,9].

To understand how different isotypes of human therapeutic antibodies alone, or in combination, can affect Fc-mediated tumoricidal functions and improve clinical efficacy, we developed a human immune-three dimensional (3D) tumor cell model as a test platform. Tumor cells grown as 3D structures (spheroids), which resemble many aspects of *in vivo* solid tumors, have greater power to predict clinical efficacies than classical monolayer assays[10,11,12]. Rituximab (RTX), a chimeric IgG1 directed to the CD20 antigen on B cells widely used in B cell malignancies and autoimmunity[13,14,15], was used as model antibody to evaluate isotype functions. The capacity of IgG1-4 and IgA1-2 variants of RTX to induce CDC, and ADP by human monocytic effector cells was evaluated using human B cell lymphomas, grown in 3D spheroids or in two dimensional (2D) monolayers as comparison, were investigated. We provide here the first functional characterizations of different RTX isotypes in 3D spheroids of B cell lymphoma and assess the potential of Fc-mediated effector functions in cancer immunotherapy.

Results

Characterization of human monocytic effector cells and B cell lymphoma target cells

A pre-clinical model was developed to evaluate how therapeutic antibodies, of different isotypes, activate the human anti-tumor immune response. Mono-Mac-6, a human $CD14^+$ monocytic cell line with functional properties of mature monocytes was selected as effector cells[16]. Following staining with FcR-specific antibodies the Mono-Mac-6 cells was evaluated for expression by flow cytometry. CD64, CD32 and CD89, but not CD16A and CD32B, were detected (Fig. 1A, B). The absence of CD32B suggests that the positive CD32 staining, detected with the IV.3 antibody, originates from the presence of CD32A on the Mono-Mac-6 cells.

To stimulate the FcRs and cytotoxicity of the effector cells, we cultured the Mono-Mac-6 cells with interferon gamma (IFN-ɣ)[17]. Indeed, IFN-ɣ improved the effector function of the Mono-Mac-6 cells mediating ADP (Supplementary Fig. 1) and was subsequently used in all ADP experiments.

As tumor target cells we used two established human $CD20^+$ B cell lymphoma cell lines, Raji and GRANTA-519[18]. CD20 expression on the target cells was verified. The expression level (median fluorescence intensity; MFI) of CD20 was comparable on Raji and GRANTA-519 cells, and a 1.95- and 2.12-fold increase in the MFI respectively was observed, in comparison to their respective isotype control (Fig. 1C).

IgG3 subclass of the RTX anti-CD20 antibody is a superior mediator of ADP

The therapeutic activity and mechanism of action of RTX IgG isotype variants (IgG1, IgG2, IgG3 and IgG4) was assessed by their ability to mediate ADP in effector cells. Raji and GRANTA-519 target cells, fluorescently labeled with carboxyfluorescein succinimidyl ester (CFSE), were incubated with either RTX-IgG1, RTX-IgG2, RTX-IgG3, RTX-IgG4 or human isotype controls in 2D cultures. Subsequently, Mono-Mac-6 cells were added and assessed for maximum phagocytosis, using different effector:target cell ratios, time points and RTX concentration, of antibody-treated tumor cells (Supplementary Fig. 2). The optimized ADP was quantified as the percentage of target cells (CFSE) phagocytosed by Mono-Mac-6 cells ($CD89^+$) by flow cytometry (Fig. 2A). One-hour co-culture of effector cells with antibody-coated target cells in a 1:1 ratio revealed that different RTX IgG subclasses have different potency in stimulating ADP. The RTX-IgG3 subclass induced the greatest ADP of tumor cells and the overall potency of isotypes in stimulating phagocytosis was RTX-IgG3>IgG1>IgG4>>>IgG2 (Fig. 2B). This RTX isotype efficacy pattern did not change when ADP was performed in the presence of human plasma (data not shown). Human isotype control antibodies did not mediate any substantial ADP and was similar to untreated target cells. ADP was subsequently verified by fluorescence confocal microscopy, which demonstrated different stages of phagocytosis by partial or complete engulfment of RTX-IgG3 opsonized Raji target cells (Fig. 2C).

To confirm a role of FcγRs in the ADP response, we used the FcγR-specific antibodies 10.1 (anti-CD64) and AT10 (anti-CD32A and B)[19] to block the effector cells prior co-culture with the RTX-opsonized target cells. In this experiment we also used the antibody IV.3 with high affinity to CD32A and with unknown blocking effect. Indeed, the phagocytosis of RTX-IgG3 opsonized Raji cells after blocking with AT10 was 29% decreased in the effector cells (12.2% ± 0.86) compared to the phagocytosis without blocking (17.17% ± 0.40) (Fig. 3). Notably, the IV.3 antibody also inhibited the phagocytosis (12.17% ± 0.45), while no effect

was observed by the anti-CD64 antibody (17.20% ± 0.96), indicating that CD32A participate in the phagocytosis in the monocytic effector cells.

RTX anti-CD20 antibody IgG2 subclass strongly enhances ADP when combined with other RTX isotypes

Synergistic effects of different RTX anti-CD20 isotypes in stimulating ADP mediated by Mono-Mac-6 effector cells must also be considered. Interestingly, when combining RTX-IgG1 (2.5 μg ml^{-1}) and RTX-IgG2 (2.5 μg ml^{-1}) (i.e. total 5 μg ml^{-1}) a 2.24 fold enhancement of the phagocytic efficacy was observed (20.40% ± 0.82), when compared to RTX-IgG1 alone in full (5 μg ml^{-1}) (9.12% ± 0.49) or half dose (2.5 μg ml^{-1}) (9.53% ± 0.72) on Raji cells (Fig. 4A). This effect was not seen when RTX-IgG1 was combined with an IgG2 isotype control antibody (9.00% ± 0.55). Likewise, when combining RTX-IgG2 with RTX-IgG3 (24.93% ± 1.13) or RTX-IgG4 (11.50% ± 0.36) ADP was greatly enhanced compared to single effect by full or half dose of RTX-IgG3 (12.3% ± 2.27 and 10.66% ± 0.49) (Fig. 4B) or RTX-IgG4 (6.03% ± 0.16 and 4.98% ± 0.11) (Fig. 4C). To investigate further if the RTX-IgG2 could be combined with isotypes other than IgG to enhance ADP, we explored the effect on RTX-IgA1 and RTX-IgA2 subclasses. RTX-IgA1 and IgA2 in half doses (2.5 μg ml^{-1}) stimulated ADP (3.24% ± 0.08 and 3.57% ± 0.60, respectively) in the Raji cell cultures in contrast to human IgA isotype control (0.69% ± 0.12) (Fig. 4D). When RTX-IgA1 or RTX-IgA2 in half doses was combined with RTX-IgG2 (2.5 μg ml^{-1}) the phagocytic capacity was enhanced (5.37% ± 0.57 and 6.07% ± 0.18, respectively) (Fig. 4D). The synergistic effect of RTX-IgG2 with other RTX-isotypes was also evident using GRANTA-519 as tumor target cells (Supplementary Fig. 3A). While RTX-IgG4 had some synergistic effects when combined with RTX-IgG3 (Supplementary Fig. 3B), dual combinations of RTX-IgG3 and RTX-IgG1 did not induce any ADP enhancing effects (Supplementary Fig. 4).

IgG2 and IgG4 isotypes of the RTX antibody have been reported to trigger apoptosis[20]. Hence, we investigated the potential contribution of CD20-mediated apoptosis to ADP enhancement by RTX-IgG2 in combination with other RTX isotype. Tumor target cells were opsonized with the different RTX-IgG isotypes alone, or in combination (RTX-IgG2 and RTX-IgG3). Lymphoma cells were thereafter stained with Annexin V and analyzed by flow cytometry. An increase in the Annexin V positive cell population was observed when target cells where opsonized with RTX-IgG2 or RTX-IgG4, but not when opsonized with RTX-IgG1 or RTX-IgG3 (Fig. 5A, B). The largest Annexin V population was induced by RTX-

IgG2. Interestingly, apoptosis could also be observed when the target cells were opsonized with RTX-IgG2 in combination with RTX-IgG3, suggesting that apoptosis could contribute to the ADP enhancing effect induced by RTX-IgG2 and RTX-IgG4 isotypes.

To verify the contribution of apoptosis in the enhancing effect of FcR-induced phagocytosis with RTX, target cells were incubated with staurosporine, a well known inducer of apoptosis. Indeed, a significant Annexin V positive population was observed in the target cells after exposure to staurosporine and an enhancement of the phagocytic efficacy by RTX-IgG3 (the isotype with best efficacy in the ADP assay). Thus, a 1.74 fold enhancement of the phagocytosis was observed when the target cells had been treated with staurosporine and RTX-IgG3 (22.47% ± 0.90) in comparison with RTX-IgG3 treated target cells (12.93% ± 0.49) (Fig. 5C).

CDC is mediated in both target cells by RTX-IgG3, while RTX-IgG1 only in Raji cells

The capacity to mediate CDC in Raji and GRANTA-519 cells was evaluated by treating target cells with single RTX-IgG isotypes in culture media supplemented with 25% human plasma (containing complement proteins). Trypan blue exclusion of target cells demonstrated high cell viability in untreated (98.44% ± 1.08) and isotype control treated cells (98.41% ± 0.97) (Fig. 6A). In contrast, RTX-IgG3 induced CDC resulting in marked decrease in cell viability in both Raji (5.03% ± 4.13) and GRANTA-519 (9.97% ± 5.38) target cells, while RTX-IgG1 triggered CDC in Raji cells only (8.33% ± 4.29) (Fig. 6A). A modest CDC was also induced by RTX-IgG2 in Raji cells (95.00% ± 1.10), whereas no CDC was observed for RTX-IgG4 (97.15% ± 2.95). The CDC triggered by RTX-IgG3 in Raji and GRANTA-519 cells was completely ablated when using heat-inactivated human plasma (data not shown), confirming the role of native complement proteins in this process. Furthermore, it was evident that the overall CDC was greater when using Raji as target cells than GRANTA-519 cells. To investigate possible mechanisms for this we analyzed target cell expression of CD59, a critical membrane complement regulator. CD59 expression is associated with inhibition of membrane attack complex formation and resistance to therapeutic antibodies, including RTX[21,22]. Interestingly, flow cytometry data showed greater CD59 expression in GRANTA-519 cells (MFI 27.30 ± 1.10 and isotype control MFI 2.00 ± 0.14) than Raji cells (MFI 3.83 ± 0.46 and isotype control MFI 1.46 ± 0.05) (Fig. 6B). This may contribute to protection against complement activation mediated by RTX-IgG1 in GRANTA-519 cells.

A human immune - 3D tumor model was developed to study ADP

The 2D monolayer cell culture of lymphoma cells showed important aspects of using different RTX isotypes to mediate particular effector functions. Nevertheless, a more predictive model to better mimic the human *in vivo* tumor environment would allow us to filter out therapeutic antibody methods for clinical success earlier. Thus, we developed a multicellular 3D tumor spheroid model. Cell culture wells were coated with a matrix of agarose facilitating Raji and GRANTA-519 lymphoma cells to form 3D spheroids (Fig. 7A). With this culture technology, the two tumor lines developed spheroids of approximately 1000 μm in size within 2-3 days (Fig. 7B). Interestingly, spheroid growth was different in the two lymphoma cell lines. Raji cells developed a more compact spheroid shape in comparison with GRANTA-519 cells, which developed spheroids of looser character.

The expression level of CD20 in the lymphoma cells was not affected by the 3D culture and showed comparable CD20 MFI (Supplementary Fig. 5), considering them suitable for immunotherapy treatment. When whole spheroids were further analyzed by confocal microscopy we observed that the CD20 antigen was heterogeneously expressed, with a prominent expression at the spheroid border (Fig. 7C, D).

Subsequently, CFSE-labeled Raji and GRANTA-519 spheroids were opsonized with RTX-IgG1 or RTX-IgG3 (the most potent isotypes in the 2D model), and co-cultured with Mono-Mac-6 ($CD89^+$) effector cells for 2 hours. When the co-cultures were investigated by fluorescence confocal microscopy it was observed that the majority of Mono-Mac-6 cells were located in the periphery of the spheroids, while some effector cells were also able to migrate to the center of the spheroids (Fig. 8A). Using novel quantitative metrics, we calculated the migration of effector cells by measuring their distance from center of RTX-IgG1 and RTX-IgG3-opsonized Raji and GRANTA-519 spheroids. Results show higher effector cell migration in RTX-IgG3 (146 pixels ± 65 from spheroid center), with the majority (42.94%) of monocytes in the second quartile, compared to RTX-IgG1 (125 pixels ± 50) opsonized Raji spheroids, which resulted in the majority (44.13%) of monocytes in the third quartile closer to the spheroid periphery. Whereas in opsonized GRANTA-519 spheroids similar effector cell migration is observed between RTX-IgG1 (209 pixels ± 82) and RTX-IgG3 (210 pixels ± 77) and showed similar distribution of monocytes (Fig. 8B).

In parallel, co-cultured spheroids were disrupted and the percentages of phagocytosed target cells by Mono-Mac-6 cells was determined by flow cytometry. Both RTX-IgG1 and RTX-IgG3 isotypes stimulated phagocytosis of spheroid cells, while isotype controls not (Fig. 8C).

RTX-IgG3 was superior in inducing ADP, both in Raji (3.30% ± 0.86) and GRANTA-519 (4.12% ± 0.07) spheroids compared to RTX-IgG1 opsonized Raji (0.92% ± 0.19) and GRANTA-519 (2.26% ± 0.38) spheroids. We next compared the capacity of all RTX isotypes to mediate ADP in the Mono-Mac-6 effector cells in the Raji 3D tumor model. Once again the RTX-IgG3 showed superior ADP activity (6.85% ± 2.03) over RTX-IgG1 (2.68% ± 0.97), which was followed by RTX-IgG4 (1.95% ± 0.63), while RTX-IgG2 triggered no ADP (0.72% ± 0.16) (similar to isotype controls), and RTX-IgA1 and RTX-IgA2 stimulated a very modest ADP (1.12% ± 0.07 and 0.91% ± 0.21 respectively) (Fig. 8D). When RTX-IgG2 was used in combination with RTX-IgG3 in the spheroids it could not enhance the ADP further (Supplementary Fig. 6).

We also determined the influence of the RTX isotypes in the ADP activity of human peripheral blood monocytes in the Raji 3D tumor model. The primary monocytes, isolated from healthy blood donors, showed CD64, CD32, CD32B, CD89 and a modest CD16A expression (Supplementary Fig. 7) and demonstrated similar ADP pattern as the Mono-Mac-6 cells to the different RTX IgG isotypes (Fig. 8D, E). Thus, the efficacy to stimulate ADP was in the following order: RTX-IgG3>RTX-IgG1>RTX-IgG4 while RTX-IgG2 did not induce any ADP (Fig. 8E). This suggests that the Mono-Mac-6 human immune – 3D tumor model is a clinical relevant model to evaluate efficacy of therapeutic IgG antibodies of different subclasses. Furthermore, and in contrast to the Mono-Mac-6 effector cells, the human primary monocytes mediated substantial phagocytosis in response to RTX-IgA1 or RTX-IgA2 opsonized spheroids (Fig. 8E). This is interesting and implies that human primary monocytes, possibly due to their high CD89 expression, are effective in responding to IgA complexes and should be considered as effector cells in the 3D tumor model when evaluating the efficacy of therapeutic IgA antibodies.

RTX isotypes capacity to mediate CDC in the 3D model is highly reduced in comparison to 2D cultures

The efficacy of RTX-IgG1 and RTX-IgG3, the most potent RTX isotypes mediating CDC in 2D cultures, were subsequently investigated in the 3D tumor model. CDC could be induced by RTX-IgG3 in Raji spheroids (66.12% cell viability ± 8.80), while RTX-IgG1 had a very modest effect (86.29% ± 13.6) when compared to isotype control (99.31% ± 0.54) (Fig. 9A). Neither RTX isotype could trigger CDC in GRANTA-519 spheroids. Notably, the CD59 expression was higher in 3D cultured cells compared to 2D cultured cells, as the MFI of the

anti-CD59 staining in Raji spheroids was 2.33 ± 0.10 and 2.13 ± 0.05 in Raji 2D cultured cells and 31.06 ± 1.20 in GRANTA-519 spheroids and 19.50 ± 1.51 in GRANTA-519 2D cultured cells (Fig. 9B). However, although CD59 was slightly upregulated in Raji spheroids it was overall lower than in GRANTA-519.

Discussion

Advanced model systems and tools for human tumor immunology are lacking and choosing the right model system for a given immunological question is essential. Current preclinical models fail to accurately predict the human outcome, mainly due to fundamental differences between the human immune system and the murine models we typically use to study anti-tumor immune responses[23]. To address this, we have developed a reproducible fully human immune-3D tumor model for drug screening. This novel 3D tumor model reflects more accurately the complex *in vivo* properties of a tumor than 2D monolayers, not least with respect to drug resistance, as spheroids are exposed to dramatically different adhesive, topographical and mechanical forces that modify their responses to various stimuli[24]. Hence, the 3D model was used in parallel with 2D cultures to explore the capacity of therapeutic antibodies of different isotypes to stimulate tumor cell killing.

A common method to investigate efficacy of antibody-based immunotherapy has been ADCC. ADCC relies on a single FcγR, CD16A, and the activity is predominantly evaluated in natural killer cells. However, macrophages have emerged as critical immune effectors of therapeutic antibodies in cancer[25,26]. They express all classes of FcγR in contrast to natural killer cells and have immense potential to destroy tumors via the process of ADP[4,7]. Human macrophages are though more difficult to study as they do not circulate in the bloodstream. On the other hand, human peripheral blood monocytes can easily be isolated and subsequently differentiated into macrophages by cytokines *ex vivo*. Nevertheless, monocytes are a heterogeneous population, and individuals can express different FcRs and display various FcR polymorphisms that can affect the outcome of mAb treatment[27,28]. To overcome this, and provide a fair comparison of isotype effector functions, we used Mono-Mac-6, an FcR-stable human monocytic cell line. Mono-Mac-6 cells exhibit many characteristics closely related to mature classical monocytes, such as expression of CD64, CD32A and CD89, which are upregulated in human monocytes under hypoxic conditions (found in tumors)[29].

To validate the clinical relevance of Mono-Mac-6 cells in the 3D tumor model we used human primary monocytes as effector cells, which carry CD64, CD32A, and CD89 as Mono-Mac-6, in addition to CD16A and CD32B. In the human-immune tumor model we also explored two different types of $CD20^+$ B cell lymphoma. This was particularly apparent in the 3D culture, as Raji cells (Burkitt lymphoma) formed more compact spheroids in comparison to GRANTA-519 cells (mantle cell lymphoma). The different physical properties of spheroids may reflect the diverse morphology of human B cell lymphoma *in vivo*[30]. Additionally, the membrane attack complex inhibitor CD59, but not the CD20 antigen, was significantly enhanced on lymphoma cells when cultured in 3D, in contrast to 2D. CD59 has previously been shown to promote tumor growth *in vivo*[31] and has been recognized as an important determinant of tumor sensitivity to RTX treatment[32,33]. This suggests that the 3D model is promising for anti-CD20 immunotherapy studies, as features associated with treatment resistance are developed, resembling the clinical situation.

RTX-IgG1 was among the first anti-CD20 mAb to be approved by the FDA for demonstrated clinical efficacy in the treatment of B-cell malignancies[6,13,32]. However, different structures and functions of human isotypes than IgG1 may be advantageous for specific indications – depending on the targeted antigen and the desired mode of action. Here we recognized that RTX-IgG1 triggered significant ADP in 2D and 3D cultures of Raji and GRANTA-519 cells, while CDC was only triggered in 2D cultures of Raji cells. RTX-IgG3 triggered higher ADP than RTX-IgG1 in both 2D and 3D cultures, and also induced CDC in tumor monolayers and in Raji spheroids. The CDC results in the 2D cultures are in line with previous studies showing that the clinical relevant RTX-IgG1 is a weaker activator of CDC than RTX-IgG3 in monolayers of B cell lymphoma[34]. Indeed, the overall capacity of RTX-IgG3 to trigger both ADP and CDC against B lymphoma was stronger than RTX-IgG1, although the efficacy in the spheroids was markedly reduced compared to monolayer cultures.

Nevertheless, greater effector cell migration was detected by imaging in the RTX-IgG3 opsonized Raji spheroids compared to RTX-IgG1, while in the more loosely GRANTA-519 spheroids the RTX isotypes had similar migration capacity. Hence, tumor structure plays a role in determining receptor expression and sensitivity to RTX treatment. The reason the IgG3 subclass of RTX is a superior mediator of ADP in opsonized tumor target cells may be due to its unique large hinge region that provides higher flexibility of the Fab arms, which in

turn influences antigen- binding ability and FcγR interaction[35]. Consistent with previous findings[19], interaction with CD32A seems to play an important role for the ADP. The strong efficiency of IgG3 to mediate CDC, via the classical pathway, may also be due to the flexibility on the Fc region provided by its hinge[21,36]. Overall, our data show IgG3 possesses superior effector functions over IgG1 that render it well for use in cancer therapy. However, owing to an enhanced susceptibility to proteolysis, shorter half-life than other IgG subclasses and aggregation during bioprocessing, IgG3 has not been used as a therapeutic drug[37]. To circumvent these obstacles engineered human IgG3 anti-CD20 antibodies containing the CH3 constant domain from IgG1 have recently been developed, providing a new arsenal of IgG3 antibodies to explore[37].

The efficacy of RTX-IgG2 to induce effector functions in the 2D and 3D lymphoma models was low. Very modest ADP and CDC were detected in Raji monolayers. These findings support Fc-mediated effector functions by IgG2 are limited[38]. Unexpectedly, when RTX-IgG2 was combined with RTX-IgG3 we observed a two-fold enhancement of the 2D ADP response in comparison to single RTX-IgG3 treatment. This enhancement was also seen when combining the RTX-IgG2 with other RTX isotypes. One possible mechanism for this enhancement could be the contribution of CD20-mediated apoptosis. It has previously been reported that higher apoptosis induction by RTX-IgG2, compared to RTX-IgG1, is due to the structural differences in the CH1 and hinge domains of the heavy chain[20]. In light with this, we could demonstrate that apoptosis induced in target cells by CD20-independent apoptosis (by staurosporine) could also enhance the ADP efficacy by RTX-IgG3. This is interesting and can have bearings on the beneficial outcome of combining chemotherapy and RTX in the treatment of many non-Hodgkin's lymphomas that have been documented up to date[39-40]. The apoptotic cell population possibly presents an "eat me" signal enhancing the phagocytic activity of monocytic effector cells when activated by antibody-binding FcγRs[41]. The synergistic effect of RTX-IgG2 to enhance ADP was not apparent in the tumor spheroids but deserves attention for further studies.

RTX-IgG4 was capable of inducing ADP in monolayers of Raji and GRANTA-519 cells, although at lower levels, and could also induce ADP in Raji spheroids. Furthermore, RTX-IgG4 triggered CD20-mediated apoptosis and could demonstrate some synergistic effect in enhancing ADP when combined with RTX-IgG3, although not as potent as RTX-IgG2. These

data highlight IgG4 as a proficient stimulator of ADP in monocytic cells to eradicate tumor cells. However, since IgG4 is a non-complement fixing subclass, also demonstrated by us by means of the lack of CDC by RTX-IgG4, its use in tumor cell killing is limited, whereas beneficial in clinical situations when complement activation is not desired.

While IgG are utmost used in antibody-based therapies, the immunotherapeutic potential of IgA antibodies remains rather unexplored. Here we demonstrate that both RTX IgA1 and IgA2 subclasses can mediate tumor cell killing in 2D cultures by Mono-Mac-6 effector cells, an effect substantially enhanced when combined with RTX-IgG2. A small ADP activity was also noted in the Mono-Mac-6 cells in response to RTX-IgA1 or RTX-IgA2 opsonized Raji spheroids. Furthermore, our results from human primary monocytes as effector cells in RTX-opsonized 3D spheroids verified the impact of IgG isotypes of inducing ADP in the order of IgG3>IgG1>IgG4 >>>IgG2, confirming the findings in Mono-Mac-6 cells, but also demonstrated substantial ADP activity by IgA isotypes. Thus, the adaptive function of CD89 appears more powerful in primary monocytes. Most studies with therapeutic IgA antibodies have utilized CD89-expressing neutrophils from healthy blood donors as effector cells to show anti-cancer efficacy by means of neutrophil-mediated ADCC[42]. Our data are thus novel showing IgA represents an alternative therapeutic isotype that can additionally perform cytotoxicity by engaging CD89-expressing monocytes for phagocytosis of aggregated tumor cells.

Only careful testing can determine which isotype fits a specific therapeutic purpose and efforts in stimulating the myeloid arm of the immune system with different mAb isotypes to attack cancers have potential to improve antibody-based immunotherapy. Thus, by employing human therapeutic IgG isotypes in the human immune-3D tumor model, we have advanced the immuno-oncology field enabling analysis of CDC, tumor cell killing by monocytes and effector cell infiltration ex vivo. This model is advantageous for many cancer forms, not only lymphoma, as tumor aggregates (3D spheroids) resemble the clinical *in vivo* situation. It is a valuable tool in research, as well as in the biotech industry in the development and selection of engineered IgG antibodies, that does not require the use of animals. Importantly, using peripheral blood monocytes as effector cells the human immune-3D tumor model can be used as a screening model to predict the patient's response to IgG or IgA-based immunotherapy, and can also be employed as an antibody drug screening platform in many cell culture laboratories.

In conclusion, our model reveals several important findings about therapeutic mAbs; IgG isotypes with selective binding to CD32A have important tumor cell killing effects by monocytic phagocytes. The IgG3 variant of RTX is the most potent isotype mediating ADP (followed by RTX-IgG1) and CDC in tumor targets. RTX-IgG4 mediates no CDC but has sufficient stimulatory activity to induce phagocytosis. RTX IgA subclasses can also mediate potent ADP, thereby representing alternative therapeutic isotypes against cancer. The choice of the FcR "inactive", but apoptotic-inducing, RTX-IgG2 in combination with other RTX isotypes can be beneficial to enhance the phagocytic activity. Similarly, RTX-stimulated phagocytosis can be enhanced by apoptosis-inducing agents. Thus, additional approaches to engage monocytes/macrophages in tumors further, apart from Fc engineering of therapeutic antibodies for greater binding to FcRs, can be advantageous.

Material and Methods

Antibodies

The RTX isotype family, monoclonal human IgG1, IgG2, IgG3, IgG4, IgA1 and IgA2 anti-human CD20, were bought from InvivoGen, Toulouse, France (cat. hcd20-mab, hcd20-mab2, hcd20-mab3, hcd20-mab4, hcd20-mab6, hcd20-mab7). Human isotype controls, IgG1 kappa, IgG2 kappa, IgG3 kappa, IgG4 kappa and IgA1 kappa were from Bio-Rad, California, USA (cat. HCA192, HCA193, HCA194, HCA195, HCA189). Monoclonal mouse IgG2a anti-human CD20 PE-conjugated (clone LT20) was from EuroBioScience, Friesoythe, Germany (cat. H12155A, cat. H12155P). Monoclonal mouse IgG1 anti-human CD89 PE-conjugated (clone A59) and monoclonal mouse IgG1 anti-human CD16 FITC-conjugated (clone 3G8) were purchased from BD, Franklin Lakes, NJ, USA (cat. 555686, 555406). Monoclonal mouse IgG1 anti-human CD64 FITC-conjugated (clone 10.1) and monoclonal mouse IgG2a anti-human CD59 PE-conjugated were from BioLegend, San Diego, CA, USA (cat. 305006, 304707). Monoclonal mouse IgG2b anti-human CD32 FITC-conjugated (clone IV.3) was from STEMCELL Technologies, Vancouver, BC, Canada (cat. 60012Fl.1). Monoclonal mouse IgG1 anti-human CD32 (clone KB61) was purchased from Dako, Santa Clara, CA (cat. M7190). Monoclonal mouse IgG2b anti-human CD32A (clone IV.3) was provided by Johan Ronnelid (Department of Immunology, Genetics and Pathology (IGP), Uppsala University, Uppsala, Sweden) and monoclonal mouse IgG1 anti-human CD32B (clone GB3) was provided by Uwe Jacob, SuppreMol, Germany.

Human plasma

Human plasma was isolated from blood, collected in heparin-coated tubes, from healthy, anonymous blood donors at the University Hospital in Uppsala, Sweden. The blood was centrifuged at 1800 rpm at room temperature for 15 min without brakes and the plasma was collected. Heat-inactivated plasma was produced by heating the plasma at 56 °C for 30 min and centrifuged thereafter for 15 min at 12,000 RCF. All plasma was stored at -80 °C for further experiments.

Isolation of primary monocytes

Peripheral blood monocytes were isolated from citrate-anticoagulated buffy coats (leukocyte concentrates) obtained from whole blood donations from healthy donors (sex and age: M26, F21, F36) at the University Hospital in Uppsala, Sweden. Briefly, peripheral blood mononuclear cells (PBMCs) were separated from the buffy coats using Ficoll-Paque Plus (GE Healthcare, cat. 17-1440-02) and standard density gradient centrifugation. The PBMCs were further washed with PBS containing 2mM of EDTA, and incubated with anti-CD14 coated magnetic beads (Miltenyi Biotec, cat. 130-050-201). Positive selection of CD14+ cells was done through magnetic cell separation. Subsequently, CD14 cells were stained with anti-human CD14 PE antibody (clone: 61D3) (Invitrogen, cat. 12-0149-41) and the purity was verified (approximately 94%) by flow cytometry. After isolation, the CD14+ primary monocytes were kept overnight in a humidified chamber at 37 °C under 5% CO_2, prior ADP assay.

Cell cultures

GRANTA-519 cells (originating from human mantle lymphoma)[43] were obtained from DSMZ, Braunschweig, Germany (cat. ACC342), Raji cells (originating from human Burkitt lymphoma)[44] were kindly provided by Fredrik Öberg (IGP, Uppsala University, Uppsala, Sweden), and Mono-Mac-6 cells (originating from human acute monocytic leukemia)[16] by Helena Jernberg Wiklund (IGP, Uppsala University, Uppsala, Sweden). Authentication of Raji and Mono-Mac-6 was performed by STR-profiling (Microsynth AG, Switzerland) and the cells were cultured in RPMI 1640 (Sigma-Aldrich, cat. R0883) containing penicillin and streptomycin (Sigma-Aldrich, cat. P4333) and GRANTA-519 cells in Dulbecco's Modified Eagle's Medium (DMEM) (Sigma-Aldrich, St. Louise, MO, USA; cat. D5796) containing L-glutamine – penicillin – streptomycin (Sigma-Aldrich, cat. G6784). All cultures were

supplemented with 10% heat inactivated fetal bovine serum (Gibco, Waltham, MA, USA; cat. 11550356). The cells were cultured in a humidified chamber at 37 °C under 5% CO_2 and were routinely tested for mycoplasma contamination using MycoAlert plus detection kit (Lonza, Basel, Switzerland; cat. LT07-701).

ADP of 2D cultures

GRANTA-519 and Raji target cells were stained with Vybrant CFDA SE Cell Tracer (CFSE) (Fisher Scientific, Waltham, MA, USA; cat. V12883) following manufacturer's instruction prior seeding for monolayers at a cell density of 50 000 or 75 000 cells/well (for ratio Effector (E): Target (T) = 1:1 or 2:1 respectively) in a round bottomed 96-well plate. After CFSE staining, target cells were incubated for 30 min at 37 °C with RTX isotype. As negative controls, untreated cells or cells treated with isotype control were used. Subsequently, Mono-Mac-6 effector cells previously stimulated with recombinant human IFN-ɣ (Bio-Rad, Hercules, CA, USA; cat. PHP050) at 0.2 µg ml^{-1} for 3h at 37 °C, were added to the RTX-opsonized target cells using two different ratio of E:T cells, 1:1 and 2:1. Opsonized target cells and Mono-Mac-6 cells were co-cultured for 1-2h at 37 °C. Cells were then collected, washed with phosphate-buffered saline (PBS) (Medicago, Quebec City, QC, Canada, cat. M09-9400-100) containing 0.5% bovine serum albumin (BSA) Fraction V (VWR, Radnor, PE, USA; cat. 422371X) and incubated with anti-CD89 PE antibody for 30 min at 4 °C in the dark to fluorescently label Mono-Mac-6 cells. Cells were thereafter washed, centrifuged and the cell pellet re-dispersed in 100-200 µl of PBS containing 0.5% BSA and the cell fluorescence intensity was measured using a MACSQuant VYB Flow Cytometer (Miltenyi Biotec, Bergisch Gladbach, Germany). A minimum of 15 000 events were analyzed for each sample. Gating of $CD89^+$ Mono-Mac-6 cells that became $CFSE^+$ were considered positive phagocytic cells. Gating strategy can be seen in supplementary figure 8, adhered to guidelines for the use of flow cytometry[45].

Staurosporine (Proteinkinase, Biaffin GmbH & Co KG, Germany; cat. PKI-STSP-001) was used as apoptosis-inducer agent and target cells were incubated with 0.5 µM of Staurosporine for 24h at 37 °C prior Annexin V staining and ADP assay.

Imaging of 2D cultures

Monolayers of opsonized CFSE-labelled target cells (Raji or GRANTA-519) and Mono-Mac-6 cells were co-cultured for 2h at 37 °C. Cells were then collected, washed with PBS

containing 0.5% BSA and incubated with anti-CD89 PE antibody and Hoechst 33342 (Invitrogen, cat. R17753) for 30 min at 4 °C. Cells were fixed with 4% paraformaldehyde (PFA) for 30 min at room temperature. Cells were then washed, centrifuged and the cell pellet re-dispersed in 50 µl of PBS containing 0.5% BSA and added into microscope slides (Superfrost Plus, ThermoScientific, Waltham, MA, USA; cat. J1800AMNZ). The co-cultured Mono-Mac-6 effector cells and RTX-opsonized target cells were imaged in glycerol at room temperature using a LSM 710 Elyra S.1, AxioObserver confocal microscope (Oberkochen, Germany) equipped with 405, 488 and 561 nm lasers and Plan-Apochromat 63x/1.4 Oil DIC M27. Images were acquired using Zen (Black edition) software and analysed using the open source Java application ImageJ (https://imagej.nih.gov/ij/).

Development of 3D tumor spheroids and ADP

Spheroids were obtained by culturing cells (Raji and GRANTA-519) on agarose-coated plates as previously described[12]. Briefly, 0.15 g of agarose was dissolved in 10 ml of a solution composed of 90% PBS and 10% incomplete cell culture medium and autoclaved. Subsequently, 50 µl were added per well of a 96-well round bottomed microtiter plate (Sarstedt, Newton, NC, USA; cat. 83.3925) under sterile conditions. Target cells were left unstained or stained with CFSE (Fisher Scientific, cat. V12883) prior seeding. Raji cells were seeded at the concentration of 5 000 cells/well and GRANTA-519 cells at 10 000 cells/well in 200 µl of complete media. After cell seeding, the 96-well plates were spin down at room temperature for 6 min at 200 RCF. Plates were then incubated in a humidified chamber at 37 °C under 5% CO_2. Morphology and size were visualized and verified using Leica DMi1 inverted microscope (Leica Microsystems, Wetzlar, Germany). Mono-Mac-6 cells and primary human monocytes were stimulated with 0.2 µg ml^{-1} of IFN-ɣ for 3h at 37 °C prior ADP experiments. For ADP experiments, RTX-opsonized CFSE-labelled Raji and GRANTA-519 spheroids were co-cultured with Mono-Mac-6 cells or primary human monocytes for 2h at 37 °C. Cells were then collected, washed with PBS containing 0.5% BSA Fraction V (VWR, Radnor, PE, USA; cat. 422371X) and incubated with anti-CD89 PE or anti-CD14 PE antibody for 30 min at 4 °C in the dark to fluorescently label Mono-Mac-6 cells or primary human monocytes, respectively. Cells were thereafter washed, centrifuged and the cell pellet re-dispersed in 100-200 µl of PBS containing 0.5% BSA and the cell fluorescence intensity was measured using a MACSQuant VYB Flow Cytometer. A

minimum of 15 000 events were analyzed for each sample. Gating of $CD89^+$ Mono-Mac-6 cells that became $CFSE^+$ were considered positive phagocytic cells.

Imaging of 3D spheroids

RTX-opsonized CFSE-labelled Raji and GRANTA-519 spheroids, co-cultured with CD89 PE-labelled Mono-Mac-6 cells for 2h, were fixed with 4% PFA for 30 min at room temperature, washed with PBS containing 0.5% BSA and carefully added on to microscope slides (Superfrost Plus, ThermoScientific, cat. J1800AMNZ). Raji and GRANTA-519 3D spheroids co-cultured with CD89 PE labelled Mono-Mac-6 cells were imaged in glycerol at room temperature using a LSM 710 Elyra S.1, AxioObserver confocal microscope equipped with 488 and 561 nm lasers and Plan-Apochromat 10x/0.3 DIC M27. Images were acquired using Zen (Black edition) software and analysed using the open source Java application ImageJ (https://imagej.nih.gov/ij/). Mono-Mac-6 infiltration and co-localization with CFSE was measured using a spheroid infiltration macro (https://github.com/J-C-Anania/Macrophage-infiltration-in-3D-tumor-model-). Briefly, this macro measures the distance of each Mono-Mac-6 ($CD89^+$, magenta) from the spheroid (CFSE, green) periphery from 3D projected z-stack images. This macro was written in ImageJ specifically for this dataset.

CDC in 2D and 3D spheroids

Monolayers of Raji or GRANTA-519 cells were seeded at a cell density of 50 000 cells/well in 50 µl of complete culture media in a 96-well plate. Cells were incubated with RTX isotypes or human isotype control antibodies using a concentration of 5 µg ml^{-1} for 30 min at 37 °C. Then 25% human plasma was added and incubated for further 30 min at 37 °C. After incubation, viable cell numbers were determined by counting the cells on a Neubauer hemocytometer using the trypan blue exclusion method. For CDC experiments in 3D spheroids, Raji or GRANTA-519 spheroids were incubated with RTX isotypes or human isotype control antibodies using a concentration of 10 µg ml^{-1} for 30 min at 37 °C. Then 25% human plasma was added and incubated for further 24h at 37 °C. After incubation, each spheroid was disaggregated, and the cell viability was determined by cell counting on a Neubauer hemocytometer using the trypan blue exclusion method.

Statistical analysis

GraphPad Prism 8 software (version 8.4.2) were used to calculate the mean plus and minus standard deviation (SD). Three biological samples per group were analyzed in each experiment, and the number of independent experiments, performed at different occasions but following same conditions, are indicated in the figure legends.

Acknowledgements

The authors thank Dr. Marika Nestor and her research group at IGP, Uppsala University, Uppsala, Sweden for helpful discussions about spheroid culture and the BioVis facility and staff, particularly Jeremy Adler for technical and image analysis assistance, Rudbeck Laboratory, Uppsala University, Uppsala, Sweden. This work was supported by The Swedish Research Council.

Data availability

The authors declare that the main data supporting the findings of this study are available within the paper and its' Supplementary Information file. Extra data are available from the corresponding author upon reasonable request.

Author contributions

S.K. conceived the initial design of the study and together with S.L. designed the experiments. S.L., J.A., A.V. and V.S. performed the experiments. S.L., J.A., and S.K. wrote and revised the manuscript.

Competing interests

The authors declare no commercial or financial conflict of interest.

References

1. Leavy, O., Therapeutic antibodies: past, present and future. *Nat. Rev. Immunol.* 2010. 10**:**297.
2. Carter, P. J. and Lazar, G. A., Next generation antibody drugs: pursuit of the 'high-hanging fruit'. *Nat. Rev. Drug Discov.* 2018. 17: 197–223.
3. Chames, P., Van Regenmortel, M., Weiss, E. and Baty, D., Therapeutic antibodies: successes, limitations and hopes for the future. *Br. J. Pharmacol.* 2009. 157: 220–233.
4. Hogarth, P. M. and Pietersz, G. A., Fc receptor-targeted therapies for the treatment of inflammation, cancer and beyond. *Nat. Rev. Drug Discov.* 2012. 11: 311–331.
5. Braster, R., O'Toole, T. and van Egmond, M., Myeloid cells as effector cells for monoclonal antibody therapy of cancer. *Methods* 2014. 65: 28–37.
6. Chenoweth, A. M., Wines, B. D., Anania, J. C. and Mark Hogarth, P., Harnessing the immune system via FcγR function in immune therapy: a pathway to next-gen mAbs. *Immunol. Cell Biol.* 2020. 98: 287–304.
7. Guilliams, M., Bruhns, P., Saeys, Y., Hammad, H. and Lambrecht, B. N., The function of Fcγ receptors in dendritic cells and macrophages. *Nat. Rev. Immunol.* 2014. 14: 94–108.
8. Valerius, T., Stockmeyer, B., van Spriel, A. B., Graziano, R. F., van den Herik-Oudijk, I. E., Repp, R., Deo, Y. M., et al., FcαRI (CD89) as a Novel Trigger Molecule for Bispecific Antibody Therapy. *Blood* 1997. 90: 4485–4492.
9. Leusen, J. H. W., IgA as therapeutic antibody. *Mol. Immunol.* 2015. 68: 35–39.
10. Weiswald, L.-B., Bellet, D. and Dangles-Marie, V., Spherical Cancer Models in Tumor Biology. *Neoplasia* 2015. 17: 1–15.
11. Fennema, E., Rivron, N., Rouwkema, J., van Blitterswijk, C. and de Boer, J., Spheroid culture as a tool for creating 3D complex tissues. *Trends Biotechnol.* 2013. 31: 108–115.
12. Friedrich, J., Seidel, C., Ebner, R. and Kunz-Schughart, L. A., Spheroid-based drug screen: considerations and practical approach. *Nat. Protoc.* 2009. 4: 309–324.
13. Pierpont, T. M., Limper, C. B. and Richards, K. L., Past, Present, and Future of Rituximab—The World's First Oncology Monoclonal Antibody Therapy. *Frontiers in Oncology* 2018. 8: 163.
14. Edwards, J. C. W., Szczepański, L., Szechiński, J., Filipowicz-Sosnowska, A., Emery, P., Close, D. R., Stevens, R. M. and Shaw, T., Efficacy of B-cell–targeted

therapy with rituximab in patients with rheumatoid arthritis. *N. Engl. J. Med.* 2004. 350: 2572–2581.

15. Mok, C. C., Rituximab for the treatment of rheumatoid arthritis: an update. *Drug Des. Devel. Ther.* 2013. 8: 87–100.
16. Ziegler-Heitbrock, H. W., Thiel, E., Fütterer, A., Herzog, V., Wirtz, A. and Riethmüller, G., Establishment of a human cell line (Mono Mac 6) with characteristics of mature monocytes. *Int. J. cancer.* 1988. 41: 456–461.
17. Van Schie, R. C., Verstraten, R. G., Van de Winkel, J. G., Tax, W. J. and de Mulder, P. H., Effect of recombinant IFN-gamma (rIFN-gamma) on the mechanism of human macrophage IgG FcRI-mediated cytotoxicity. rIFN-gamma decreases inhibition by cytophilic human IgG and changes the cytolytic mechanism. *J. Immunol*. 1992. 148: 169-76.
18. Quentmeier, H., Pommerenke, C., Dirks, W. G., Eberth, S., Koeppel, M., MacLeod, R. A. F., Nagel, S. et al., The LL-100 panel: 100 cell lines for blood cancer studies. *Sci. Rep.* 2019. 9: 8218.
19. Richards, J. O., Karki, S., Lazar, G. A., Chen, H., Dang, W. and Desjarlais, J.R., Optimization of antibody binding to FcγRIIa enhances macrophage phagocytosis of tumor cells. *Mol. Cancer Ther.* 2008. 7: 2517 LP – 2527.
20. Könitzer, J. D., Sieron, A., Wacker, A. and Enenkel, B., Reformatting Rituximab into Human IgG2 and IgG4 Isotypes Dramatically Improves Apoptosis Induction In Vitro. *PLoS One* 2015. 10: e0145633–e0145633.
21. Fishelson, Z. and Kirschfink, M., Complement C5b-9 and Cancer: Mechanisms of Cell Damage, Cancer Counteractions, and Approaches for Intervention. *Frontiers in Immunology* 2019. 10: 752.
22. Golay, J., Lazzari, M., Facchinetti, V., Bernasconi, S., Borleri, G., Barbui, T., Rambaldi, A. and Introna, M., CD20 levels determine the in vitro susceptibility to rituximab and complement of B-cell chronic lymphocytic leukemia: further regulation by CD55 and CD59. *Blood* 2001. 98: 3383–3389.
23. Sanmamed, M. F., Chester, C., Melero, I. and Kohrt, H., Defining the optimal murine models to investigate immune checkpoint blockers and their combination with other immunotherapies. *Ann. Oncol.* 2016. 27: 1190–1198.
24. Baker, B. M. and Chen, C. S., Deconstructing the third dimension – how 3D culture microenvironments alter cellular cues. *J. Cell Sci.* 2012. 125: 3015 LP – 3024.

25. Weiskopf, K. and Weissman, I. L., Macrophages are critical effectors of antibody therapies for cancer. *MAbs* 2015. 7: 303–310.

26. Lehmann, B., Biburger, M. , Brückner, C. , Ipsen-Escobedo, A. , Gordan, S. , Lehmann, C. , Voehringer, D. et al., Tumor location determines tissue-specific recruitment of tumor-associated macrophages and antibody-dependent immunotherapy response. *Sci. Immunol.* 2017. 2: eaah6413.

27. Weng, W.-K. and Levy, R., Two Immunoglobulin G Fragment C Receptor Polymorphisms Independently Predict Response to Rituximab in Patients With Follicular Lymphoma. *J. Clin. Oncol.* 2003. 21: 3940–3947.

28. Cartron, G., Dacheux, L., Salles, G., Solal-Celigny, P., Bardos, P., Colombat, P. and Watier H., Therapeutic activity of humanized anti-CD20 monoclonal antibody and polymorphism in IgG Fc receptor FcγRIIIa gene. *Blood* 2002. 99: 754–758.

29. Bosco, M. C., Puppo, M., Santangelo, C., Anfosso, L., Pfeffer, U., Fardin, P., Battaglia, F. and Varesio L., Hypoxia modifies the transcriptome of primary human monocytes: modulation of novel immune-related genes and identification of CC-chemokine ligand 20 as a new hypoxia-inducible gene. *J. Immunol.* 2006. 177: 1941–1955.

30. Kim, H. and Dorfman, R. F., Morphological studies of 84 untreated patients subjected to laparotomy for the staging of non-Hodgkin's lymphomas. *Cancer* 1974. 33: 657–674.

31. Ouyang, Q., Zhang, L., Jiang, Y., Ni, X., Chen, S., Ye, F., Du, Y. et al., The membrane complement regulatory protein CD59 promotes tumor growth and predicts poor prognosis in breast cancer. *Int. J. Oncol.* 2016. 48: 2015–2024.

32. Boross, P. and Leusen, J. H. W., Mechanisms of action of CD20 antibodies. *Am. J. Cancer Res.* 2012. 2: 676–690.

33. Hu, W., Ge, X., You, T., Xu, T., Zhang, J., Wu, G., Peng, Z. et al., Human CD59 inhibitor sensitizes rituximab-resistant lymphoma cells to complement-mediated cytolysis. *Cancer Res.* 2011. 71: 2298–2307.

34. Rösner, T., Derer, S., Kellner, C., Dechant, M., Lohse, S., Vidarsson, G., Peipp, M. and Valerius, T., An IgG3 switch variant of rituximab mediates enhanced complement- dependent cytotoxicity against tumour cells with low CD20 expression levels. *Br. J. Haematol.* 2013. 161: 282-286.

35. Damelang, T., Rogerson, S. J., Kent, S. J. and Chung, A. W., Role of IgG3 in

Infectious Diseases. *Trends Immunol.* 2019. 40: 197–211.

36. Golay, J. and Introna, M., Mechanism of action of therapeutic monoclonal antibodies: Promises and pitfalls of in vitro and in vivo assays. *Arch. Biochem. Biophys.* 2012. 526: 146–153.
37. Saito, S., Namisaki, H., Hiraishi, K., Takahashi, N. and Iida, S., A stable engineered human IgG3 antibody with decreased aggregation during antibody expression and low pH stress. *Protein Sci.* 2019. 28: 900–909.
38. Salfeld, J. G., Isotype selection in antibody engineering. *Nat. Biotechnol.* 2007. 25: 1369–1372.
39. Habermann, T. M., Weller E. A., Morrison, V. A., Gascoyne, R. D., Cassileth, P. A., Cohn, J. B., Dakhil, S. R. et al., Rituximab-CHOP versus CHOP alone or with maintenance rituximab in older patients with diffuse large B-cell lymphoma. *J. Clin. Oncol*. 2006. 24: 3121-3127.
40. Minard-Colin, V., Aupérin, A., Pillon, M., Burke, A., Barkauskas, D. A., Wheatley, K., Delgado, R. F. et al., Rituximab for High-Risk, Mature B-Cell Non-Hodgkin's Lymphoma in Children. *N. Engl. J. Med*. 2020. 382: 2207-2219.
41. Trahtemberg, U. and Mevorach, D., Apoptotic Cells Induced Signaling for Immune Homeostasis in Macrophages and Dendritic Cells. *Front. Immunol.* 2017. 8: 1356.
42. van Egmond, M. and Bakema, J. E., Neutrophils as effector cells for antibody-based immunotherapy of cancer. *Semin. Cancer Biol.* 2013. 23: 190–199.
43. Drexler, H. G. and MacLeod, R. A. F., Malignant hematopoietic cell lines: in vitro models for the study of mantle cell lymphoma. *Leuk. Res.* 2002. 26: 781–787.
44. Epstein, M. A., Achong, B. G, Barr, Y. M., Zajac, B., Henle, G. and Henle, W., Morphological and virological investigations on cultured Burkitt tumor lymphoblasts (strain Raji). *J. Natl. Cancer Inst.* 1966. 37: 547–559.
45. Cossarizza, A., Chang, H. D., Radbruch, A., Acs, A., Adam, D., Adam- Klages, S., Agace, W. W. et al., Guidelines for the use of flow cytometry and cell sorting in immunological studies (second edition). *Eur. J. Immunol*. 2019. 49: 1457–1973.

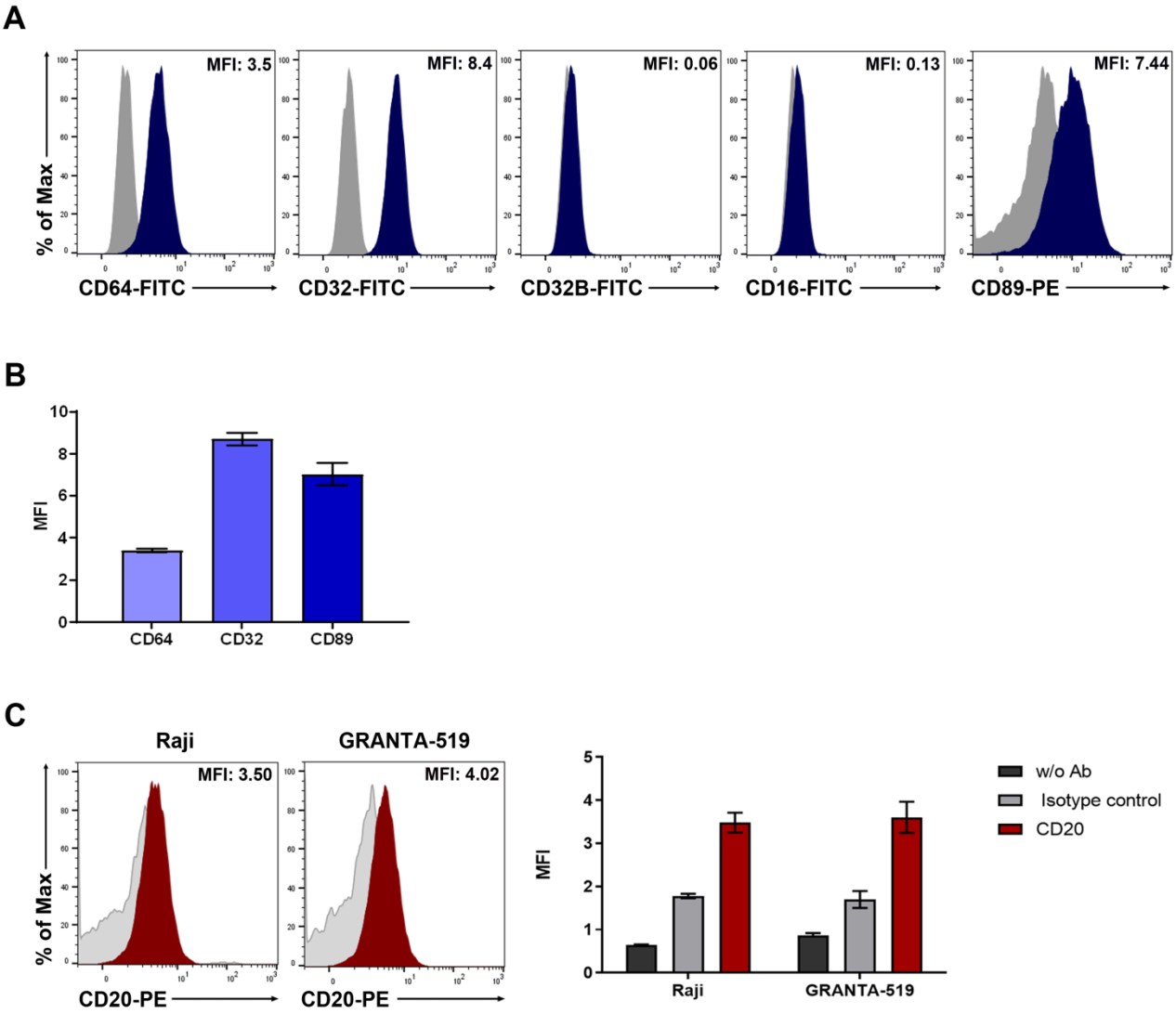

Fig. 1. Characterization of effector cells and tumor target cells. A) Representative histograms of Mono-Mac-6 effector cells stained with anti-CD64 (FITC), anti-CD32 (FITC), anti-CD32B (FITC), anti-CD16 (FITC) and anti-CD89 (PE) antibodies. Grey histograms represent isotype control and blue histograms Fc receptor staining. The median fluorescence intensity (MFI) of Fc receptors, obtained by subtracting the MFI of the isotype control, is indicated in each histogram . B) FcR expression in Mono-Mac-6 cells displayed as the mean of the MFI with corresponding isotype control subtracted ± SD of three biological samples (n=3) from one representative out of three independent experiments. C) Representative histograms of Raji and GRANTA-519 target cells stained with anti-CD20 (PE) antibody. Grey histograms represent isotype control and red histograms CD20 staining. The MFI of CD20 (without isotype MFI subtracted) is indicated in each histogram. Bar charts display the mean MFI ± SD of CD20 expression

in target cells of three biological samples per group (n=3) from one representative out of three independent experiments. w/o Ab = without antibody (unstained). All data were measured by flow cytometry.

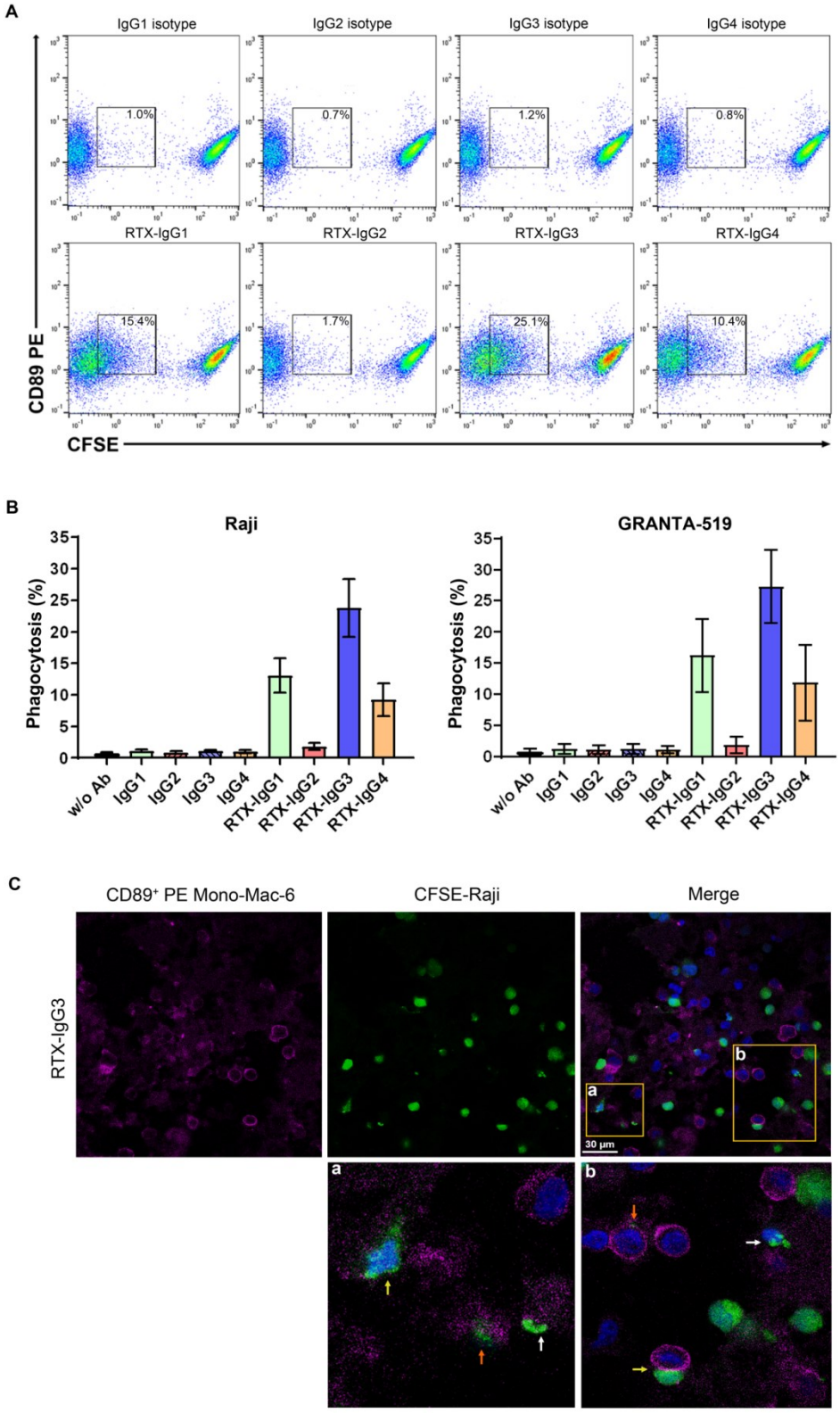

Fig. 2. RTX isotype-mediated ADP of target cells. A) Representative flow cytometry dot plots showing percentage phagocytosis of RTX opsonized CFSE-labelled Raji cells cultured in monolayers by PE anti-CD89 labelled Mono-Mac-6 effector cells at a 1:1 effector:target (E:T) cell ratio. Phagocytosis was quantified as the percentage of double positive $CFSE^+$ $CD89^+$ (PE) Mono-Mac-6 cells (square gate). B) Bar graph representation of percentage phagocytosis of Raji and GRANTA-519 cells by Mono-Mac-6 cells induced by single RTX isotype or isotype control Ab. Data are presented as the mean percentage phagocytosis ± SD of three independent experiments (n=3), each experiment performed with three biological samples per group. C) Representative confocal image z-stack projection of Mono-Mac-6 effector cells (PE $CD89^+$, magenta) phagocytosing RTX-IgG3 opsonized Raji cells (CFSE, green), co-stained for nuclei (Hoechst, blue). Insets (a, b) show the different phases of phagocytosis observed (arrows); early (yellow), intermediate (white), and late phase (orange) in the MonoMac-6 effector cells. One representative image from three independent experiments is shown. Scale bar = 30 µm, magnification 63x.

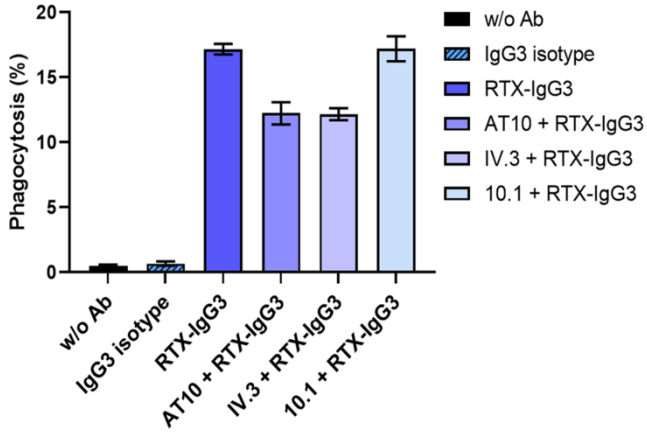

Fig. 3. FcγR blocking of effector cells and ADP. Mono-Mac-6 cells were incubated with the FcγR-specific antibodies AT10 (anti-CD32), IV.3 (anti-CD32) or 10.1 (anti-CD64) prior co-culture with RTX-IgG3 opsonized Raji target cells cultured in monolayers. Phagocytosis of target cells by Mono-Mac-6 was quantified by flow cytometry. Data are presented as the mean percentage phagocytosis ± SD of three biological samples (n=3) from one representative out of three independent experiments.

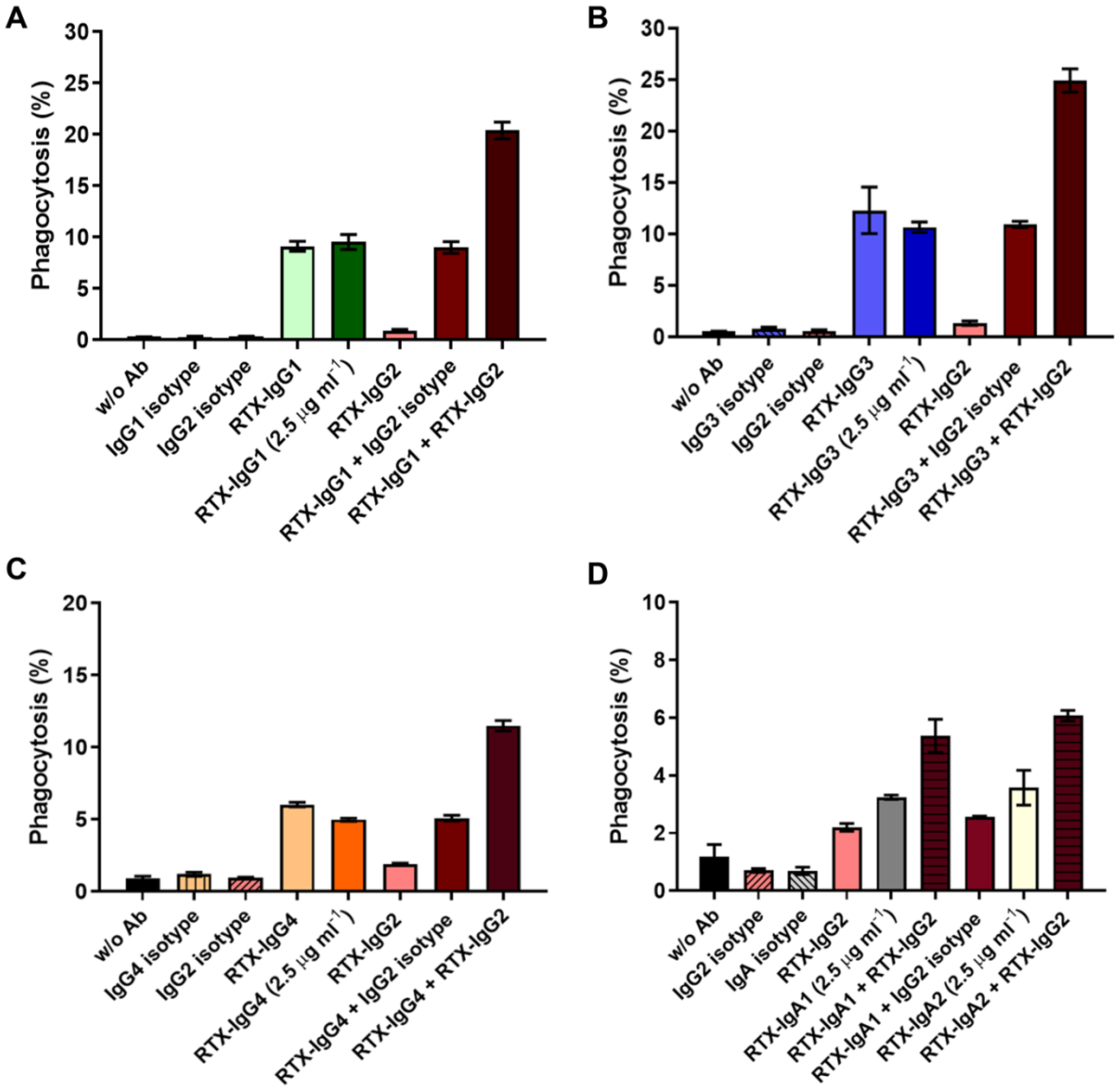

Fig. 4. ADP mediated by single or dual combinations of RTX- isotypes. Phagocytosis of RTX-IgG2 opsonized Raji cells cultured in monolayers, in combination with A) RTX-IgG1, B) RTX-IgG3, C) RTX-IgG4, D) RTX-IgA1 or RTX-IgA2 by Mono-Mac-6 effector cells. Single antibodies and isotype controls were used at the concentration 5 µg ml^{-1} (full dose) if not stated 2.5 µg ml^{-1} (half dose). In dual combinations each antibody was used at 2.5 µg ml^{-1}; in total representing the full dose (5 µg ml^{-1}). Data are presented as the mean percentage phagocytosis ± SD of three biological samples (n=3) from one representative out of three independent experiments. All data were measured by flow cytometry.

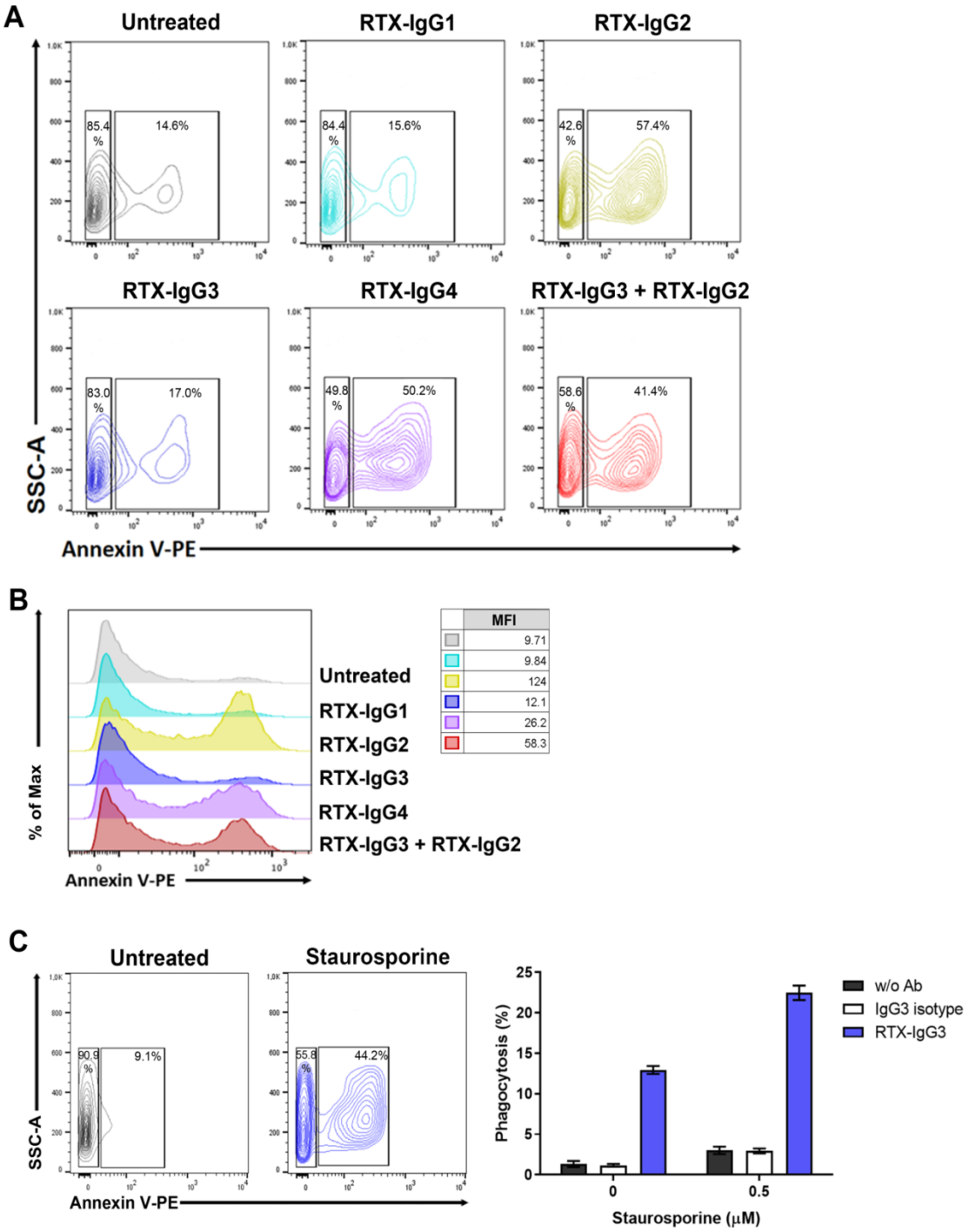

Fig. 5. Analysis of cellular apoptosis in target cells opsonized with different RTX isotypes and ADP. Representative A) contour plots and B) histograms of Annexin V PE staining in GRANTA-519 cells opsonized with single RTX isotypes or in dual combination. Cells without RTX treatment (untreated) have been used as control. Results from one representative experiment out of three are shown. Median fluorescence intensity (MFI) of Annexin V PE is indicated for each group. C) Representative contour plots of Annexin V PE staining in GRANTA-519 cells with or

without treatment of Staurosporine (0.5 µM) (left panel) and phagocytosis of RTX-IgG3 opsonized GRANTA-519 cells with or without Staurosporine treatment by Mono-Mac-6 effector cells (right panel). Bar chart displays the mean percentage of phagocytosis ± SD of three biological samples (n=3) from one representative out of three independent experiments. All data were measured by flow cytometry.

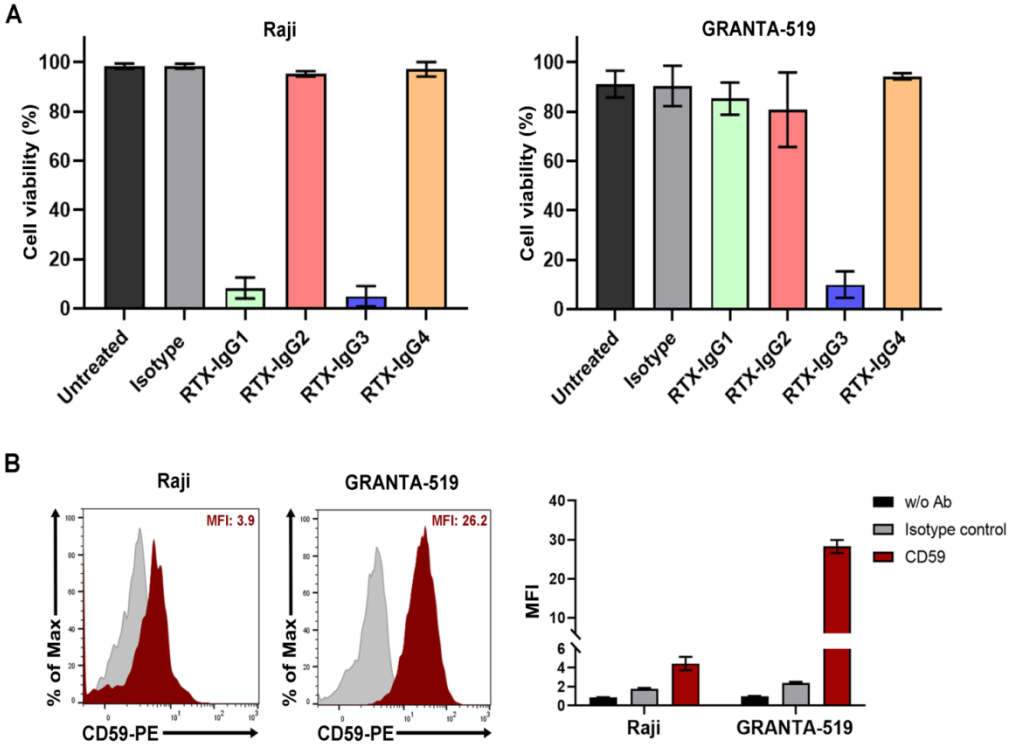

Fig. 6. CDC and CD59 expression in target cells. A) Percentage of viable Raji and GRANTA-519 cells in monolayer cultures following treatment with RTX-IgG isotypes or isotype control in media supplemented with 25% human plasma using trypan blue exclusion. Data are presented as the mean percentage cell viability ± SD of three independent experiments (n=3), each experiment performed with three biological samples per group. B) Representative histograms of Raji and GRANTA-519 cells stained with anti-CD59 PE antibody and measured by flow cytometry. Grey histograms represent isotype control and red histograms CD59 staining. The median fluorescence intensity (MFI) of CD59 is indicated in each histogram. Bar charts represent the MFI ± SD of three biological samples per group (n=3) from one representative out of three independent experiments. w/o Ab = without antibody (unstained).

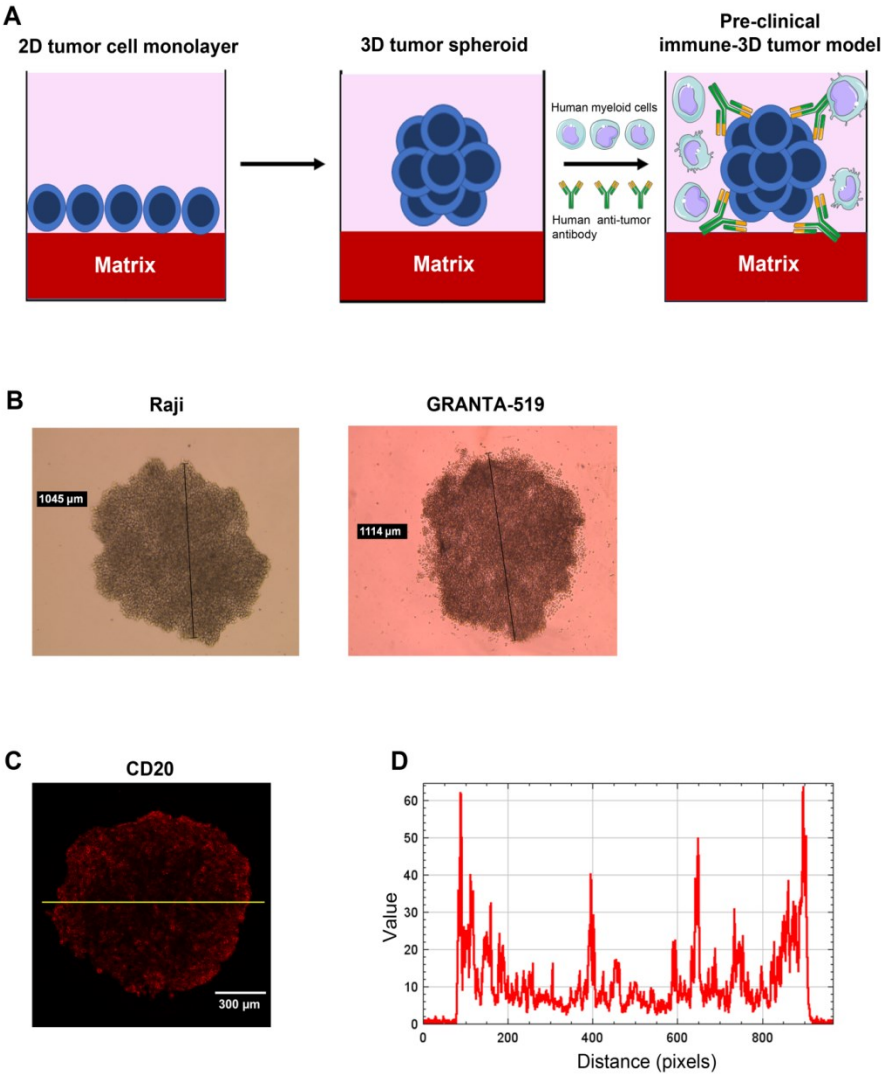

Fig. 7. Development of 3D spheroids of B cell lymphomas. A) Sketch of the development of the human immune-3D tumor model; 2D monolayers of B cell lymphoma were grown on a matrix of agarose and 2 days later a spheroid was formed. The spheroid was opsonized with therapeutic antibody and co-cultured with human monocytic effector cells to investigate tumor cell killing. B) Inverted microscopy images of cultured 3D tumor spheroids of Raji (1045 µm diameter) and GRANTA-519 (1114 µm diameter) cells after 2 days of assembly (magnification 5x). C) Confocal image z-stack projection of Raji 3D spheroid stained with PE anti-CD20 antibody (red) (scale bar = 300 µm, magnification 10x). Image is representative of three independent experiments of CD20 expression. D) Profile of CD20 intensity in Raji spheroid stained (yellow line in C). The x-axis represents distance along the spheroid and the y-axis the pixel intensity.

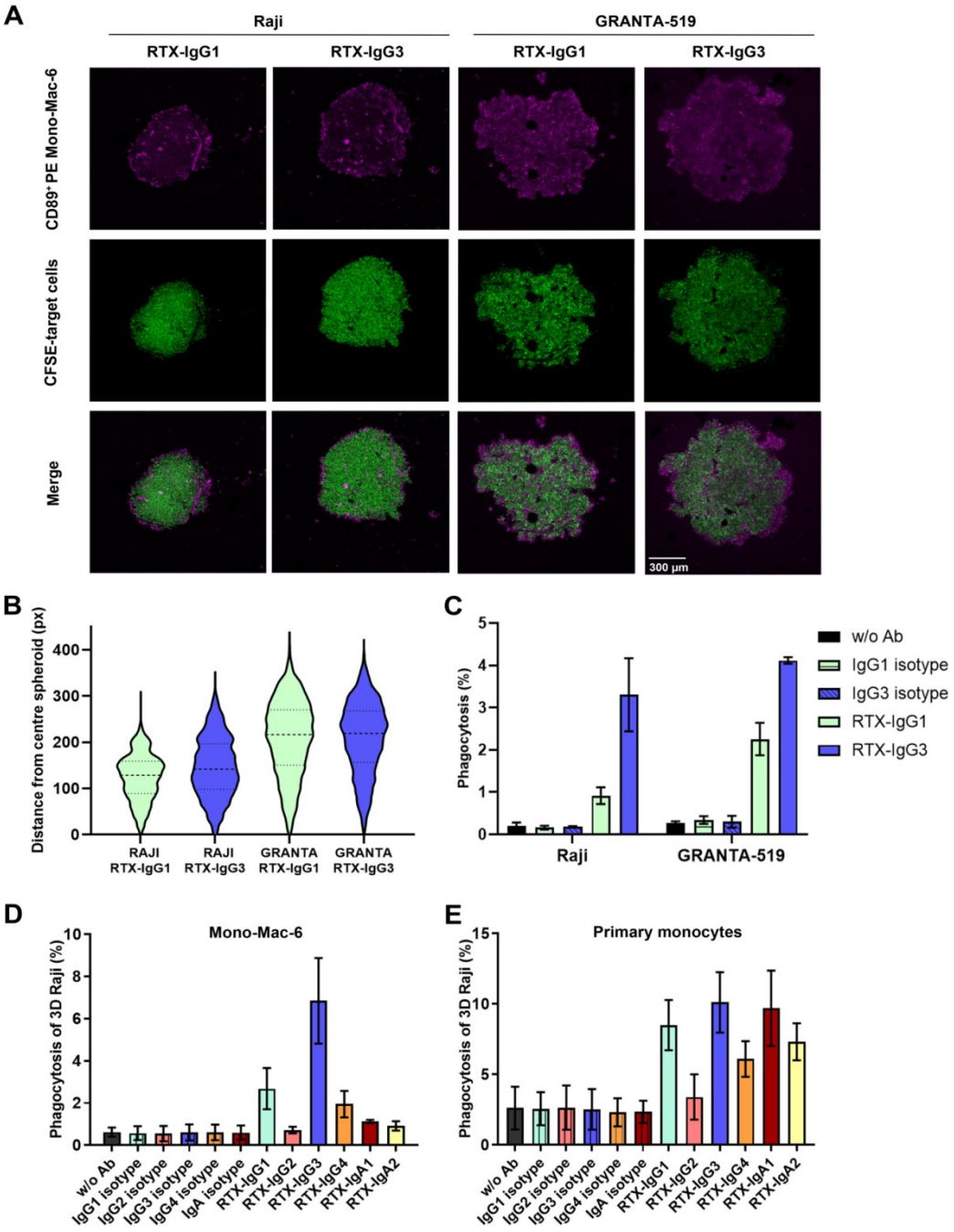

Fig. 8. ADP of spheroids opsonized with RTX isotypes. A) Z-projected confocal images of Mono-Mac-6 cells effector cells stained with anti-CD89 PE (magenta) and RTX-IgG3 or RTX-IgG1 opsonized Raji and GRANTA519 spheroids stained with CFSE (green). Results are from one representative experiment out of three. Scale bar = 300 µm, magnification 10x. B) Migration of effector cells measured by distance from the center of the spheroid (represented as 0 in the Y-axis) to the outer layer in RTX-IgG3 and RTX-IgG1 opsonized Raji and GRANTA-519 spheroids (px = pixels). Data presented as mean distance ± SD of three pooled from 3 independent experiments (n=3). C)

Phagocytosis of Raji and GRANTA-519 spheroids opsonized with RTX-IgG1 or RTX-IgG3 analyzed by flow cytometry. Data presented as mean percentage phagocytosis ± SD of three biological samples (n=3) from one representative out of three independent experiments. D) Phagocytosis of Raji spheroids by Mono-Mac-6 cells analyzed by flow cytometry and presented as mean ± SD of three independent experiments (n=3), each experiment performed with three biological samples per group. E) Phagocytosis of Raji spheroids by peripheral blood monocytes analyzed by flow cytometry and presented as mean ± SD of three independent experiments from 3 blood donors (n=3) using three biological samples per group.

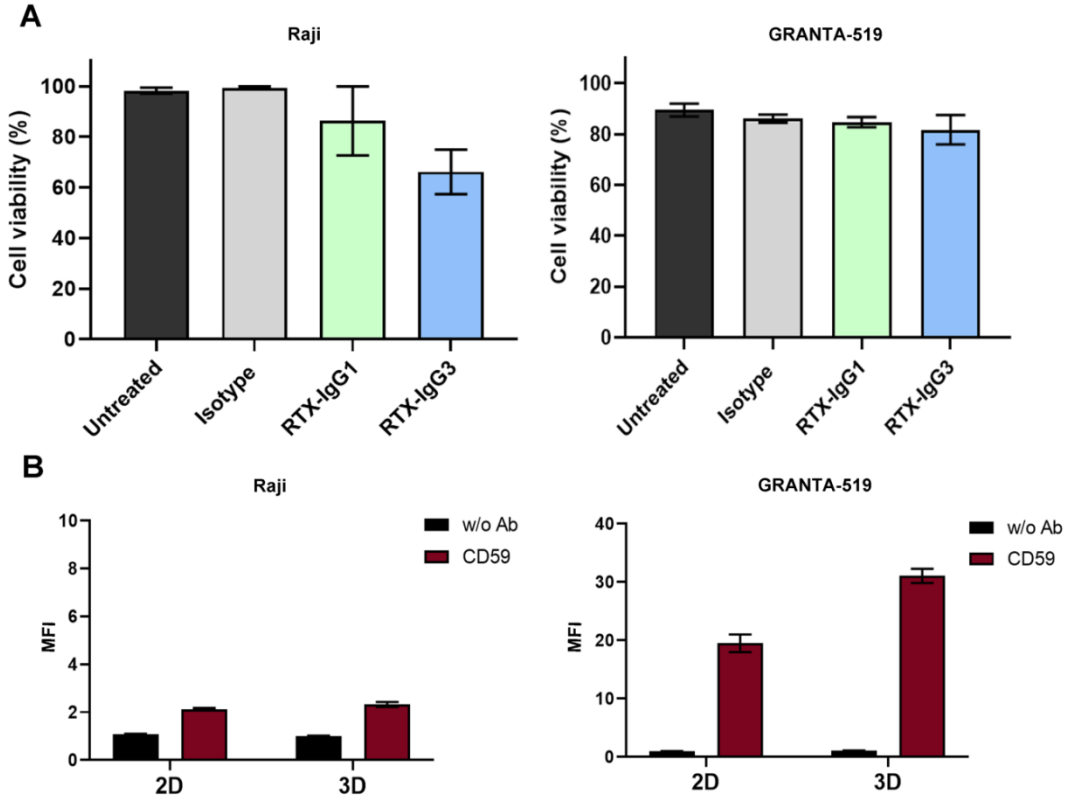

Fig. 9. CDC in spheroids and CD59 expression in 2D and 3D tumor cell cultures. A) Percentage of viable Raji cells and GRANTA-519 cells in 3D (spheroids) cultures following treatment with RTX isotypes or isotype control in media supplemented with 25% human plasma using trypan blue exclusion. Data are presented as mean percentage cell viability ± SD of three independent experiments (n=3), each experiment performed with three biological samples per group. B) CD59 expression in Raji and GRANTA-519 target cells in 2D and 3D cultures analyzed by flow cytometry. Bar charts represents the mean of median fluorescence intensity (MFI) ± SD of three biological samples (n=3) from one representative out of three independent experiments.

Graphical abstract

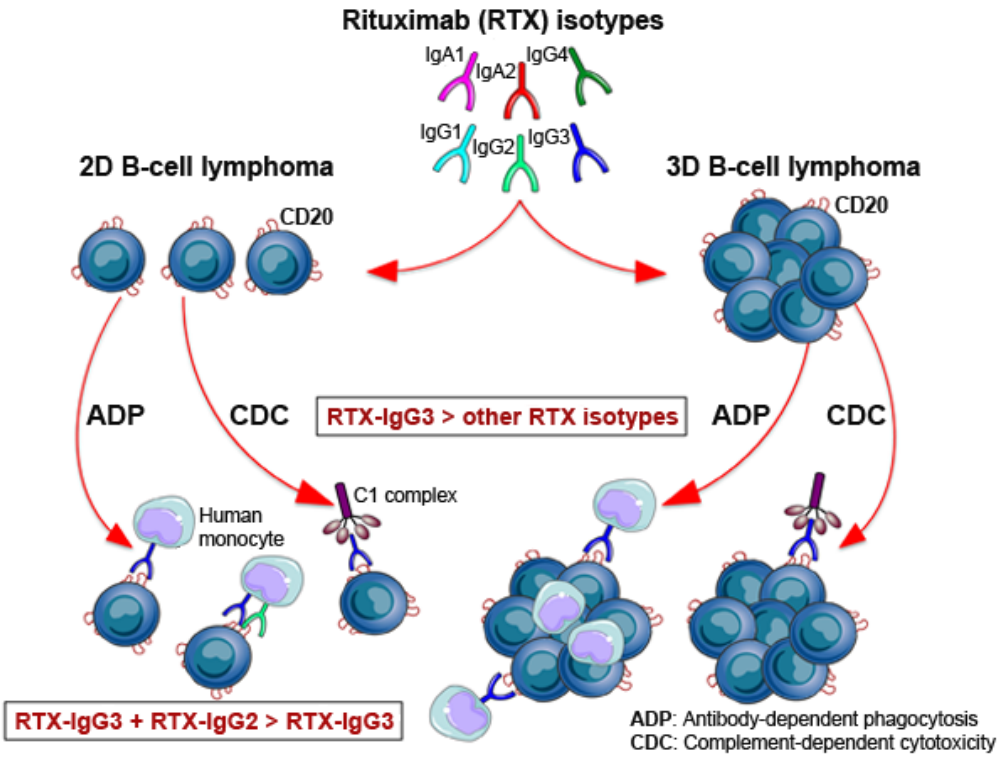

Rituximab (RTX) isotypes mediate different anti-tumor efficacy demonstrated in human 2D and 3D B-cell lymphoma models. RTX-IgG3 has the highest capacity to induce ADP in human monocytes and CDC in 2D and 3D tumor models. Addition of RTX-IgG2 to any RTX isotype greatly enhance ADP in 2D cultured lymphoma cells.